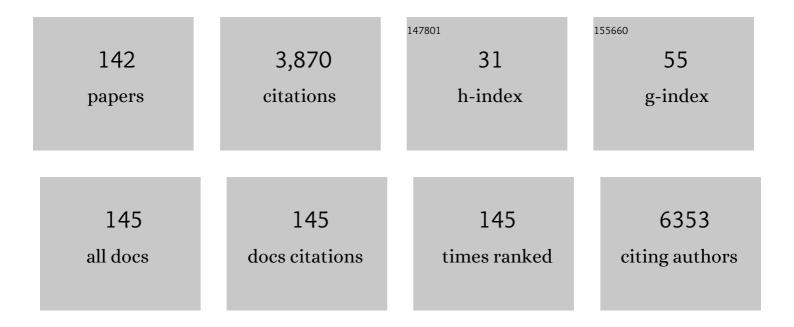
## Seung Hong Choi

List of Publications by Year in descending order

Source: https://exaly.com/author-pdf/1909718/publications.pdf Version: 2024-02-01



#	Article	IF	CITATIONS
1	Body CT and PET/CT detection of extracranial lymphoma in patients with newly diagnosed central nervous system lymphoma. Neuro-Oncology, 2022, 24, 482-491.	1.2	3
2	Myelin Content in Mild Traumatic Brain Injury Patients with Post-Concussion Syndrome: Quantitative Assessment with a Multidynamic Multiecho Sequence. Korean Journal of Radiology, 2022, 23, 226.	3.4	2
3	Prediction of hemorrhagic complications after ultrasound-guided biopsy of the thyroid and neck. European Radiology, 2022, , 1.	4.5	1
4	Response prediction of vestibular schwannoma after gamma-knife radiosurgery using pretreatment dynamic contrast-enhanced MRI: a prospective study. European Radiology, 2022, 32, 3734-3743.	4.5	2
5	Tumor-associated macrophages in cancer: recent advancements in cancer nanoimmunotherapies. Journal of Experimental and Clinical Cancer Research, 2022, 41, 68.	8.6	115
6	Risk Stratification to Define the Role of Radiotherapy for Benign and Atypical Meningioma: A Recursive Partitioning Analysis. Neurosurgery, 2022, 90, 619-626.	1.1	4
7	No Prognostic Impact of Staging Brain MRI in Patients with Stage IA Non–Small Cell Lung Cancer. Radiology, 2022, 303, 632-643.	7.3	3
8	Added Value of Contrast Leakage Information over the CBV Value of DSC Perfusion MRI to Differentiate between Pseudoprogression and True Progression after Concurrent Chemoradiotherapy in Glioblastoma Patients. Investigative Magnetic Resonance Imaging, 2022, 26, 10.	0.4	1
9	Radiological assessment schedule for high-grade glioma patients during the surveillance period using parametric modeling. Neuro-Oncology, 2021, 23, 837-847.	1.2	9
10	H3 G34-mutant high-grade glioma. Brain Tumor Pathology, 2021, 38, 4-13.	1.7	33
11	Tumor Stiffness Measurements on MR Elastography for Single Nodular Hepatocellular Carcinomas Can Predict Tumor Recurrence After Hepatic Resection. Journal of Magnetic Resonance Imaging, 2021, 53, 587-596.	3.4	21
12	Long-Term Outcomes and Sequelae Analysis of Intracranial Germinoma: Need to Reduce the Extended-Field Radiotherapy Volume and Dose to Minimize Late Sequelae. Cancer Research and Treatment, 2021, 53, 983-990.	3.0	8
13	Radiological assessment schedule for 1p/19q-codeleted gliomas during the surveillance period using parametric modeling. Neuro-Oncology Advances, 2021, 3, vdab069.	0.7	0
14	Comparison of Genetic Profiles and Prognosis of High-Grade Gliomas Using Quantitative and Qualitative MRI Features: A Focus on G3 Gliomas. Korean Journal of Radiology, 2021, 22, 233.	3.4	6
15	Blood-Brain Barrier Disruption in Mild Traumatic Brain Injury Patients with Post-Concussion Syndrome: Evaluation with Region-Based Quantification of Dynamic Contrast-Enhanced MR Imaging Parameters Using Automatic Whole-Brain Segmentation. Korean Journal of Radiology, 2021, 22, 118.	3.4	10
16	Prediction of Prognosis in Glioblastoma Using Radiomics Features of Dynamic Contrast-Enhanced MRI. Korean Journal of Radiology, 2021, 22, 1514.	3.4	21
17	Prognostic Prediction Based on Dynamic Contrast-Enhanced MRI and Dynamic Susceptibility Contrast-Enhanced MRI Parameters from Non-Enhancing, T2-High-Signal-Intensity Lesions in Patients with Glioblastoma. Korean Journal of Radiology, 2021, 22, 1369.	3.4	7
18	Clinical and Genomic Characteristics of Adult Diffuse Midline Glioma. Cancer Research and Treatment, 2021, 53, 389-398.	3.0	14

#	Article	IF	CITATIONS
19	Magnetic Resonance Imaging Parameters for Noninvasive Prediction of Epidermal Growth Factor Receptor Amplification in Isocitrate Dehydrogenase-Wild-Type Lower-Grade Gliomas: A Multicenter Study. Neurosurgery, 2021, 89, 257-265.	1.1	11
20	Differentiation between glioblastoma and primary CNS lymphoma: application of DCE-MRI parameters based on arterial input function obtained from DSC-MRI. European Radiology, 2021, 31, 9098-9109.	4.5	12
21	Multiparametric magnetic resonance imaging features of a canine glioblastoma model. PLoS ONE, 2021, 16, e0254448.	2.5	1
22	Deep Learning for Detection of Pulmonary Metastasis on Chest Radiographs. Radiology, 2021, 301, 455-463.	7.3	19
23	Revisiting vimentin: a negative surrogate marker of molecularly defined oligodendroglioma in adult type diffuse glioma. Brain Tumor Pathology, 2021, 38, 271-282.	1.7	4
24	The substantial loss of H3K27me3 can stratify risk in grade 2, but not in grade 3 meningioma. Human Pathology, 2021, 115, 96-103.	2.0	13
25	Prediction of brain age from routine T2-weighted spin-echo brain magnetic resonance images with a deep convolutional neural network. Neurobiology of Aging, 2021, 105, 78-85.	3.1	12
26	Contrast-enhanced MRI T1 Mapping for Quantitative Evaluation of Putative Dynamic Glymphatic Activity in the Human Brain in Sleep-Wake States. Radiology, 2021, 300, 661-668.	7.3	40
27	Cerebrovascular Reservoir and Arterial Transit Time Changes Assessed by Acetazolamide-Challenged Multi-Phase Arterial Spin Labeling Perfusion MRI in Chronic Cerebrovascular Steno-Occlusive Disease. Journal of the Korean Society of Radiology, 2021, 82, 626.	0.2	1
28	The Emerging Role of Fast MR Techniques in Traumatic Brain Injury. Investigative Magnetic Resonance Imaging, 2021, 25, 76.	0.4	1
29	Computed tomography complements ultrasound for the differential diagnosis of traumatic neuroma from recurrent tumor in patients with postoperative thyroid cancer. European Radiology, 2021, , 1.	4.5	3
30	Reduced Brainstem Volume After Mild Traumatic Brain Injury. American Journal of Physical Medicine and Rehabilitation, 2021, 100, 473-482.	1.4	6
31	Arterial spin labeling perfusion-weighted imaging aids in prediction of molecular biomarkers and survival in glioblastomas. European Radiology, 2020, 30, 1202-1211.	4.5	25
32	Revascularization Evaluation in Adult-Onset Moyamoya Disease after Bypass Surgery: Superselective Arterial Spin Labeling Perfusion MRI Compared with Digital Subtraction Angiography. Radiology, 2020, 297, 630-637.	7.3	14
33	Improving the Reliability of Pharmacokinetic Parameters at Dynamic Contrast-enhanced MRI in Astrocytomas: A Deep Learning Approach. Radiology, 2020, 297, 178-188.	7.3	15
34	<p>Prediction of Amyloid Positivity in Mild Cognitive Impairment Using Fully Automated Brain Segmentation Software</p> . Neuropsychiatric Disease and Treatment, 2020, Volume 16, 1745-1754.	2.2	10
35	Machine Learning Model to Predict Pseudoprogression Versus Progression in Glioblastoma Using MRI: A Multi-Institutional Study (KROG 18-07). Cancers, 2020, 12, 2706.	3.7	21
36	Added Value of Computed Tomography to Ultrasonography for Assessing LN Metastasis in Preoperative Patients with Thyroid Cancer: Node-by-Node Correlation. Cancers, 2020, 12, 1190.	3.7	12

#	Article	IF	CITATIONS
37	Diagnostic Accuracy and Confidence of [18F] FDG PET/MRI in comparison with PET or MRI alone in Head and Neck Cancer. Scientific Reports, 2020, 10, 9490.	3.3	17
38	A glioneuronal tumor with CLIP2-MET fusion. Npj Genomic Medicine, 2020, 5, 24.	3.8	3
39	Growth and Clinical Impact of 6-mm or Larger Subsolid Nodules after 5 Years of Stability at Chest CT. Radiology, 2020, 295, 448-455.	7.3	27
40	Radiomics prognostication model in glioblastoma using diffusion- and perfusion-weighted MRI. Scientific Reports, 2020, 10, 4250.	3.3	50
41	Prognostication of anaplastic astrocytoma patients: application of contrast leakage information of dynamic susceptibility contrast-enhanced MRI and dynamic contrast-enhanced MRI. European Radiology, 2020, 30, 2171-2181.	4.5	7
42	Positional effect of preoperative neuronavigational magnetic resonance image on accuracy of posterior fossa lesion localization. Journal of Neurosurgery, 2020, 133, 546-555.	1.6	6
43	Intracranial Metaplastic Meningioma : Clinical and Radiological Characteristics of 11 Cases. Journal of Korean Neurosurgical Society, 2020, 63, 657-663.	1.2	5
44	Ultrasonographic Indeterminate Lymph Nodes in Preoperative Thyroid Cancer Patients: Malignancy Risk and Ultrasonographic Findings Predictive of Malignancy. Korean Journal of Radiology, 2020, 21, 598.	3.4	18
45	Prognostic Value of Dynamic Contrast-Enhanced MRI-Derived Pharmacokinetic Variables in Glioblastoma Patients: Analysis of Contrast-Enhancing Lesions and Non-Enhancing T2 High-Signal Intensity Lesions. Korean Journal of Radiology, 2020, 21, 707.	3.4	8
46	Quantitative dynamic contrast-enhanced MR imaging shows widespread blood-brain barrier disruption in mild traumatic brain injury patients with post-concussion syndrome. European Radiology, 2019, 29, 1308-1317.	4.5	26
47	Increased Antiangiogenic Effect by Blocking CCL2-dependent Macrophages in a Rodent Glioblastoma Model: Correlation Study with Dynamic Susceptibility Contrast Perfusion MRI. Scientific Reports, 2019, 9, 11085.	3.3	48
48	Altered Vascular Permeability in Migraine-associated Brain Regions: Evaluation with Dynamic Contrast-enhanced MRI. Radiology, 2019, 292, 713-720.	7.3	23
49	Decreased APE-1 by Nitroxoline Enhances Therapeutic Effect in a Temozolomide-resistant Glioblastoma: Correlation with Diffusion Weighted Imaging. Scientific Reports, 2019, 9, 16613.	3.3	8
50	Deep Learning for Chest Radiograph Diagnosis in the Emergency Department. Radiology, 2019, 293, 573-580.	7.3	107
51	Prediction of IDH genotype in gliomas with dynamic susceptibility contrast perfusion MR imaging using an explainable recurrent neural network. Neuro-Oncology, 2019, 21, 1197-1209.	1.2	80
52	The Korean Society for Neuro-Oncology (KSNO) Guideline for Glioblastomas: Version 2018.01. Brain Tumor Research and Treatment, 2019, 7, 1.	1.0	19
53	Clinical observation of lymphopenia in patients with newly diagnosed glioblastoma. Journal of Neuro-Oncology, 2019, 143, 321-328.	2.9	34
54	Assessment of Early Therapeutic Response to Nitroxoline in Temozolomide-Resistant Glioblastoma by Amide Proton Transfer Imaging: A Preliminary Comparative Study with Diffusion-weighted Imaging. Scientific Reports, 2019, 9, 5585.	3.3	11

#	Article	IF	CITATIONS
55	Evaluation of Tumor Blood Flow Using Alternate Ascending/Descending Directional Navigation in Primary Brain Tumors: A Comparison Study with Dynamic Susceptibility Contrast Magnetic Resonance Imaging. Korean Journal of Radiology, 2019, 20, 275.	3.4	2
56	The Effect of Varying Slice Thickness and Interslice Gap on T <sub>1</sub> and T <sub>2</sub> Measured with the Multidynamic Multiecho Sequence. Magnetic Resonance in Medical Sciences, 2019, 18, 126-133.	2.0	13
57	Diagnostic value of computed tomography combined with ultrasonography in detecting cervical recurrence in patients with thyroid cancer. Head and Neck, 2019, 41, 1206-1212.	2.0	2
58	The Korean Society for Neuro-Oncology (KSNO) Guideline for WHO Grade II Cerebral Gliomas in Adults: Version 2019.01. Brain Tumor Research and Treatment, 2019, 7, 74.	1.0	7
59	Application of Vendor-Neutral Iterative Reconstruction Technique to Pediatric Abdominal Computed Tomography. Korean Journal of Radiology, 2019, 20, 1358.	3.4	23
60	The Korean Society for Neuro-Oncology (KSNO) Guideline for WHO Grade III Cerebral Gliomas in Adults: Version 2019.01. Brain Tumor Research and Treatment, 2019, 7, 63.	1.0	8
61	Leakage correction improves prognosis prediction of dynamic susceptibility contrast perfusion MRI in primary central nervous system lymphoma. Scientific Reports, 2018, 8, 456.	3.3	7
62	Improving Arterial Spin Labeling by Using Deep Learning. Radiology, 2018, 287, 658-666.	7.3	73
63	Evaluation of lymphedema in upper extremities by MR lymphangiography: Comparison with lymphoscintigraphy. Magnetic Resonance Imaging, 2018, 49, 63-70.	1.8	41
64	Monitoring Cerebral Perfusion Changes after Revascularization in Patients with Moyamoya Disease by Using Arterial Spin-labeling MR Imaging. Radiology, 2018, 288, 565-572.	7.3	54
65	Radiogenomics correlation between MR imaging features and major genetic profiles in glioblastoma. European Radiology, 2018, 28, 4350-4361.	4.5	63
66	Differentiation of High-Grade from Low-Grade Astrocytoma: Improvement in Diagnostic Accuracy and Reliability of Pharmacokinetic Parameters from DCE MR Imaging by Using Arterial Input Functions Obtained from DSC MR Imaging. Radiology, 2018, 286, 981-991.	7.3	20
67	T1 Shortening in the Globus Pallidus after Multiple Administrations of Gadobutrol: Assessment with a Multidynamic Multiecho Sequence. Radiology, 2018, 287, 258-266.	7.3	32
68	Seronegative granulomatosis with polyangiitis presenting with multiple cranial nerve palsies. Neuropathology, 2018, 38, 192-197.	1.2	4
69	Loss of Pericytes in Radiation Necrosis after Glioblastoma Treatments. Molecular Neurobiology, 2018, 55, 4918-4926.	4.0	16
70	Radiogenomics Profiling for Clioblastoma-related Immune Cells Reveals CD49d Expression Correlation with MRI parameters and Prognosis. Scientific Reports, 2018, 8, 16022.	3.3	25
71	Persistent/Recurrent Differentiated Thyroid Cancer: Clinical and Radiological Characteristics of Persistent Disease and Clinical Recurrence Based on Computed Tomography Analysis. Thyroid, 2018, 28, 1490-1499.	4.5	10
72	Application of Synthetic MRI for Direct Measurement of Magnetic Resonance Relaxation Time and Tumor Volume at Multiple Time Points after Contrast Administration: Preliminary Results in Patients with Brain Metastasis. Korean Journal of Radiology, 2018, 19, 783.	3.4	16

#	Article	IF	CITATIONS
73	Can Amide Proton Transfer MRI Distinguish Benign and Malignant Head and Neck Tumors?. Radiology, 2018, 288, 791-792.	7.3	6
74	Quantitative radiomic profiling of glioblastoma represents transcriptomic expression. Oncotarget, 2018, 9, 6336-6345.	1.8	16
75	Arterial spin labeling. Neurology India, 2018, 66, 283.	0.4	1
76	Prognosis prediction of non-enhancing T2 high signal intensity lesions in glioblastoma patients after standard treatment: application of dynamic contrast-enhanced MR imaging. European Radiology, 2017, 27, 1176-1185.	4.5	27
77	A subpopulation of cancer stem cells identifies radiographic characteristics in glioblastoma. Oncology Letters, 2017, 13, 1175-1182.	1.8	2
78	Dynamic contrast-enhanced MR imaging in predicting progression of enhancing lesions persisting after standard treatment in glioblastoma patients: a prospective study. European Radiology, 2017, 27, 3156-3166.	4.5	27
79	Comparison between the Prebolus T1 Measurement and the Fixed T1 Value in Dynamic Contrast-Enhanced MR Imaging for the Differentiation of True Progression from Pseudoprogression in Glioblastoma Treated with Concurrent Radiation Therapy and Temozolomide Chemotherapy. American Journal of Neuroradiology, 2017, 38, 2243-2250.	2.4	20
80	Glutaminase 2 expression is associated with regional heterogeneity of 5-aminolevulinic acid fluorescence in glioblastoma. Scientific Reports, 2017, 7, 12221.	3.3	23
81	Recursive partitioning analysis for disease progression in adult intracranial ependymoma patients. Journal of Clinical Neuroscience, 2017, 46, 72-78.	1.5	3
82	Temporal bone chondroblastoma: Imaging characteristics with pathologic correlation. Head and Neck, 2017, 39, 2171-2179.	2.0	12
83	BCAT1 is a New MR Imaging-related Biomarker for Prognosis Prediction in IDH1-wildtype Glioblastoma Patients. Scientific Reports, 2017, 7, 17740.	3.3	20
84	DDIS-04. NITROXOLINE EXHIBIT ANTICANCER ACTIVITY INDUCING APOPTOSIS IN AÂTEMOZOLOMIDE-RESISTANT GLIOBLASTOMA. Neuro-Oncology, 2017, 19, vi59-vi59.	1.2	0
85	Application of Cardiac Gating to Improve the Reproducibility of Intravoxel Incoherent Motion Measurements in the Head and Neck. Magnetic Resonance in Medical Sciences, 2017, 16, 190-202.	2.0	14
86	The frequency and prognostic effect of TERT promoter mutation in diffuse gliomas. Acta Neuropathologica Communications, 2017, 5, 62.	5.2	71
87	Combined use of susceptibility weighted magnetic resonance imaging sequences and dynamic susceptibility contrast perfusion weighted imaging to improve the accuracy of the differential diagnosis of recurrence and radionecrosis in high-grade glioma patients. Oncotarget, 2017, 8, 20340-20353.	1.8	15
88	Post-bevacizumab Clinical Outcomes and the Impact of Early Discontinuation of Bevacizumab in Patients with Recurrent Malignant Glioma. Cancer Research and Treatment, 2017, 49, 129-140.	3.0	5
89	Underexpression of HOXA11 Is Associated with Treatment Resistance and Poor Prognosis in Glioblastoma. Cancer Research and Treatment, 2017, 49, 387-398.	3.0	41
90	MR Imaging Analysis of Non-Measurable Enhancing Lesions Newly Appearing after Concomitant Chemoradiotherapy in Glioblastoma Patients for Prognosis Prediction. PLoS ONE, 2016, 11, e0166096.	2.5	9

#	Article	IF	CITATIONS
91	Ultrasonographic Differentiation Between Nodular Hyperplasia and Neoplastic Follicular-Patterned Lesions of the Thyroid Gland. Ultrasound in Medicine and Biology, 2016, 42, 1816-1824.	1.5	9
92	T1-Weighted MR imaging of liver tumor by gadolinium-encapsulated glycol chitosan nanoparticles without non-specific toxicity in normal tissues. Nanoscale, 2016, 8, 9736-9745.	5.6	23
93	The survival significance of a measurable enhancing lesion after completing standard treatment for newly diagnosed glioblastoma. Journal of Clinical Neuroscience, 2016, 34, 145-150.	1.5	1
94	Application of diffusion-weighted imaging and dynamic susceptibility contrast perfusion-weighted imaging for ganglioglioma in adults: Comparison study with oligodendroglioma. Journal of Neuroradiology, 2016, 43, 331-338.	1.1	10
95	Metabolomic analysis of percutaneous fine-needle aspiration specimens of thyroid nodules: Potential application for the preoperative diagnosis of thyroid cancer. Scientific Reports, 2016, 6, 30075.	3.3	36
96	Off-site evaluation of three-dimensional ultrasound for the diagnosis of thyroid nodules: comparison with two-dimensional ultrasound. European Radiology, 2016, 26, 3353-3360.	4.5	15
97	Capability of arterial spin labeling MR imaging in localizing seizure focus in clinical seizure activity. European Journal of Radiology, 2016, 85, 1295-1303.	2.6	46
98	Predictors of survival for patients with cancer after cryptogenic stroke. Journal of Neuro-Oncology, 2016, 128, 277-284.	2.9	30
99	Monitoring Cerebrovascular Reactivity through the Use of Arterial Spin Labeling in Patients with Moyamoya Disease. Radiology, 2016, 278, 205-213.	7.3	40
100	On the Utility of Short Echo Time (TE) Single Voxel 1H–MRS in Non–Invasive Detection of 2–Hydroxyglutarate (2HG); Challenges and Potential Improvement Illustrated with Animal Models Using MRUI and LCModel. PLoS ONE, 2016, 11, e0147794.	2.5	10
101	Assessment of bevacizumab resistance increased by expression of BCAT1 in IDH1 wild-type glioblastoma: application of DSC perfusion MR imaging. Oncotarget, 2016, 7, 69606-69615.	1.8	11
102	Sclerosing Meningioma : Radiological and Clinical Characteristics of 21 Cases. Journal of Korean Neurosurgical Society, 2016, 59, 584.	1.2	4
103	<i><scp>IDH2</scp></i> mutation in gliomas including novel mutation. Neuropathology, 2015, 35, 236-244.	1.2	19
104	Hemodynamic Significance of Internal Carotid or Middle Cerebral Artery Stenosis Detected on Magnetic Resonance Angiography. Yonsei Medical Journal, 2015, 56, 1686.	2.2	5
105	Mechanism for enhanced 5-aminolevulinic acid fluorescence in isocitrate dehydrogenase 1 mutant malignant gliomas. Oncotarget, 2015, 6, 20266-20277.	1.8	38
106	Prediction of Response to Concurrent Chemoradiotherapy with Temozolomide in Glioblastoma: Application of Immediate Post-Operative Dynamic Susceptibility Contrast and Diffusion-Weighted MR Imaging. Korean Journal of Radiology, 2015, 16, 1341.	3.4	16
107	Bright Vessel Appearance on Arterial Spin Labeling MRI for Localizing Arterial Occlusion in Acute Ischemic Stroke. Stroke, 2015, 46, 564-567.	2.0	43
108	Efficacy and Safety of Radiofrequency Ablation for Treatment of Locally Recurrent Thyroid Cancers Smaller than 2 cm. Radiology, 2015, 276, 909-918.	7.3	108

#	Article	IF	CITATIONS
109	Polymeric Embolization Coil of Bilayered Polyvinyl Alcohol Strand for Therapeutic Vascular Occlusion: A Feasibility Study in Canine Experimental Vascular Models. Journal of Vascular and Interventional Radiology, 2015, 26, 117-123.	0.5	2
110	Glioblastoma Treated with Concurrent Radiation Therapy and Temozolomide Chemotherapy: Differentiation of True Progression from Pseudoprogression with Quantitative Dynamic Contrast-enhanced MR Imaging. Radiology, 2015, 274, 830-840.	7.3	102
111	Usefulness of Core Needle Biopsy for Thyroid Nodules with Macrocalcifications: Comparison with Fine-Needle Aspiration. Thyroid, 2015, 25, 657-664.	4.5	37
112	Early cognitive function tests predict early progression in glioblastoma. Neuro-Oncology Practice, 2015, 2, 137-143.	1.6	14
113	Paradoxical perfusion metrics of high-grade gliomas with an oligodendroglioma component: quantitative analysis of dynamic susceptibility contrast perfusion MR imaging. Neuroradiology, 2015, 57, 1111-1120.	2.2	9
114	Hollow MnOxPy and Pt/MnOxPy yolk/shell nanoparticles as a T1 MRI contrast agent. Journal of Colloid and Interface Science, 2015, 439, 134-138.	9.4	7
115	MR Imaging Evaluation of Intracerebral Hemorrhages and T2 Hyperintense White Matter Lesions Appearing after Radiation Therapy in Adult Patients with Primary Brain Tumors. PLoS ONE, 2015, 10, e0136795.	2.5	9
116	Contrast-Enhanced FLAIR (Fluid-Attenuated Inversion Recovery) for Evaluating Mild Traumatic Brain Injury. PLoS ONE, 2014, 9, e102229.	2.5	25
117	Prognosis Prediction of Measurable Enhancing Lesion after Completion of Standard Concomitant Chemoradiotherapy and Adjuvant Temozolomide in Glioblastoma Patients: Application of Dynamic Susceptibility Contrast Perfusion and Diffusion-Weighted Imaging. PLoS ONE, 2014, 9, e113587.	2.5	15
118	A Case Report of Preoperative and Postoperative 7.0T Brain MRI in a Patient with a Small Cell Glioblastoma. Journal of Korean Medical Science, 2014, 29, 1012.	2.5	1
119	Prognosis of Glioblastoma With Oligodendroglioma Component is Associated With the IDH1 Mutation and MGMT Methylation Status. Translational Oncology, 2014, 7, 712-719.	3.7	13
120	Segmentation-Based MR Attenuation Correction Including Bones Also Affects Quantitation in Brain Studies: An Initial Result of <sup>18</sup> F-FP-CIT PET/MR for Patients with Parkinsonism. Journal of Nuclear Medicine, 2014, 55, 1617-1622.	5.0	24
121	Organized Hematoma Developed after Suboccipital Craniectomy. , 2014, 24, 610-612.		1
122	Magnetic Resonance Imaging Diagnosis of Metastatic Lymph Nodes in a Rabbit Model: Efficacy of PJY10, a New Ultrasmall Superparamagnetic Iron Oxide Agent, with Monodisperse Iron Oxide Core and Multiple-Interaction Ligands. PLoS ONE, 2014, 9, e107583.	2.5	6
123	Glioma: Application of Whole-Tumor Texture Analysis of Diffusion-Weighted Imaging for the Evaluation of Tumor Heterogeneity. PLoS ONE, 2014, 9, e108335.	2.5	159
124	Differentiation of True Recurrence from Delayed Radiation Therapy-related Changes in Primary Brain Tumors Using Diffusion-weighted Imaging, Dynamic Susceptibility Contrast Perfusion Imaging, and Susceptibility-weighted Imaging. Journal of the Korean Society of Magnetic Resonance in Medicine, 2014, 18, 120.	0.1	0
125	Optimization of ultrasmall superparamagnetic iron oxide (P904)-enhanced magnetic resonance imaging of lymph nodes: initial experience in a mouse model. Anticancer Research, 2014, 34, 5389-96.	1.1	2
126	Post-bevacizumab treatment and clinical outcomes in recurrent malignant glioma Journal of Clinical Oncology, 2013, 31, 2098-2098.	1.6	0

#	Article	IF	CITATIONS
127	Abstract TMP39: Identifying Cerebrovascular Reserve Capacity by Arterial Spin Labeling MR in Patients with Moyamoya Disease. Stroke, 2013, 44, .	2.0	0
128	Synthesis of Uniformly Sized Manganese Oxide Nanocrystals with Various Sizes and Shapes and Characterization of Their <i>T</i> <sub>1</sub> Magnetic Resonance Relaxivity. European Journal of Inorganic Chemistry, 2012, 2012, 2148-2155.	2.0	71
129	Multifunctional mesoporous silica nanocomposite nanoparticles for pH controlled drug release and dual modal imaging. Journal of Materials Chemistry, 2011, 21, 16869.	6.7	78
130	Transformation of hydrophobic iron oxide nanoparticles to hydrophilic and biocompatible maghemite nanocrystals for use as highly efficient MRI contrast agent. Journal of Materials Chemistry, 2011, 21, 11472.	6.7	49
131	Comparison of lymph node metastases assessment With the use of USPIOâ€enhanced MR imaging at 1.5 T versus 3.0 T in a rabbit model. Journal of Magnetic Resonance Imaging, 2010, 31, 134-141.	3.4	9
132	Contrast-Enhanced MR Imaging of Lymph Nodes in Cancer Patients. Korean Journal of Radiology, 2010, 11, 383.	3.4	23
133	Nonblinking and Nonbleaching Upconverting Nanoparticles as an Optical Imaging Nanoprobe and T1 Magnetic Resonance Imaging Contrast Agent. Advanced Materials, 2009, 21, 4467-4471.	21.0	548
134	Hepatocellular Carcinoma in Liver Transplantation Candidates: Detection with Gadobenate Dimeglumine–Enhanced MRI. American Journal of Roentgenology, 2008, 191, 529-536.	2.2	82
135	Lymph Node Metastasis: Ultrasmall Superparamagnetic Iron Oxide–enhanced MR Imaging versus PET/CT in a Rabbit Model. Radiology, 2007, 242, 137-143.	7.3	37
136	Cervical Lymph Node Metastases: MR Imaging of Gadofluorine M and Monocrystalline Iron Oxide Nanoparticle–47 in a Rabbit Model of Head and Neck Cancer. Radiology, 2006, 241, 753-762.	7.3	29
137	Differentiating Malignant from Benign Common Bile Duct Stricture with Multiphasic Helical CT. Radiology, 2005, 236, 178-183.	7.3	107
138	Postbiopsy Splenic Bleeding in a Dog Model: Comparison of Cauterization, Embolization, and Plugging of the Needle Tract. American Journal of Roentgenology, 2005, 185, 878-884.	2.2	23
139	Relationship Between Various Patterns of Transient Increased Hepatic Attenuation on CT and Portal Vein Thrombosis Related to Acute Cholecystitis. American Journal of Roentgenology, 2004, 183, 437-442.	2.2	28
140	Intussusception in Adults: From Stomach to Rectum. American Journal of Roentgenology, 2004, 183, 691-698.	2.2	92
141	Preoperative Magnetic Resonance Imaging Staging of Uterine Cervical Carcinoma. Journal of Computer Assisted Tomography, 2004, 28, 620-627.	0.9	86
142	Hepatocellular Carcinoma Supplied by Portal Flow After Repeated Transcatheter Arterial Chemoembolization. American Journal of Roentgenology, 2003, 181, 889-890.	2.2	9